Modified Nonlinear Active Disturbance Rejection Control for PMSM Speed Regulation With Frequency Domain Analysis

Qiankang Hou, Yuefei Zuo, *Member, IEEE*, Jinlin Sun, Christopher H. T. Lee, *Senior Member, IEEE*, Youyi Wang, and Shihong Ding, *Member, IEEE*

***Abstract*—Strong robustness and smooth speed are two crucial goals of the high-performance permanent magnet synchronous motor (PMSM) drive systems. Conventional active disturbance rejection control (ADRC) strategy generally increases the bandwidth of the extended state observer (ESO) to improve the unsatisfactory disturbance rejection ability, which will inevitably amplify the measurement noise. To address this tough issue, a nonlinear extended state observer (NESO) using finite-time technique is constructed in this article to enhance the anti-disturbance property. On this basis, the NESO with small bandwidth is sufficient to guarantee strong robustness without sacrificing noise suppression performance. Utilizing the frequency-sweep method, the advantages of the proposed NESO-based modified ADRC (MADRC) system can be analyzed in terms of frequency domain characteristics, which is more practical than traditional theoretical analysis from a mathematical point of view. Meanwhile, a quasi-resonant controller is combined with MADRC system to attenuate the main harmonic component of torque ripple for smooth speed. Experimental results are carried out to verify the effectiveness of the proposed control scheme and frequency-sweep analysis method.**

***Index Terms*—Frequency-sweep method, nonlinear extended state observer (NESO), permanent magnet synchronous motor (PMSM), quasi-resonant (QR) controller, torque ripple suppression.**

I. Introduction

OWING to the unique features such as high efficiency, lofty torque-to-inertia ratio and simple structure, permanent magnet synchronous motor (PMSM) has been applied in the fields of robotics, computer numerical control machines, and large-scale systems, etc. [1], [2], [3]. The speed regulation control is an important operating mode of PMSM system in these industrial applications. Since the outer speed-loop generally provides the reference signal for the inner current loop, it has a significant influence on the entire drive system. As a classical control strategy, linear proportional-integral (PI) control has been widely utilized in speed control. However, simple PI control is difficult to provide desired control performance in the presence of various disturbance including cogging torque, parameter uncertainties, and flux harmonics [4].

In order to achieve high-precision speed reference tracking and excellent disturbance rejection performance, various well-known two-degree-of-freedom (2-DOF) control methods are employed in speed control [5], [6]. The fundamental idea of 2-DOF control method is to treat the internal and external disturbance as a lumped disturbance term. Then, an observer is utilized to estimate the lumped disturbance and compensate the estimation value to the feedback controller. As described in [7], the disturbance observer (DOB) was first put forward by Ohnishi in the early 1980s to estimate the external disturbance in servo motors. Unfortunately, some system states are unmeasurable in practical applications, and only estimating the disturbance is not sufficient to meet the requirements of high-performance control. To estimate the system states and disturbance simultaneously, the extended state observer (ESO) was proposed by Han in the late 1990s [8]. On this basis, the widely used active disturbance rejection control (ADRC) method is constructed based on the combination of ESO and feedback controller, which breaks through the limitations of conventional proportional-integral-derivative (PID) control [9], [10].

The application of ADRC strategy in PMSM speed control has drawn increasing attentions. Since the theoretical analysis and parameter tuning of the original ADRC are extremely complicated, the parameterized linear ADRC was adopted in [11] to compensate the parameter uncertainties and load torque. Comparative results show that the robustness of ADRC system is better than linear PI. Generally, increasing the bandwidth of ESO can improve the low-frequency disturbance rejection property, but the bandwidth is restricted by measurement noise and system stiffness [12]. To enhance the anti-disturbance performance of conventional ADRC system, a phase-locked loop

Manuscript received 7 November 2022; revised 13 February 2023; accepted 23 March 2023. Date of publication 28 March 2023; date of current version 19 May 2023. This work was supported in part by the National Science Foundation of China under Grant 61973142, in part by the Jiangsu Province and Education Ministry Co-sponsored Synergistic Innovation Center of Modern Agricultural Equipment under Grant XTCX2015 and in part by the China Scholarship Council, China under Grant 202008320567. Recommended for publication by Associate Editor A. M. Bazzi. *(Corresponding authors: Christopher H. T. Lee; Shihong Ding.)*

Qiankang Hou, Jinlin Sun, and Shihong Ding are with the School of Electrical and Information Engineering, Jiangsu University, Zhenjiang 212013, China (e-mail: houqiankang@hotmail.com; jsun@ujs.edu.cn; dsh@ujs.edu.cn).

Yuefei Zuo, Christopher H. T. Lee, and Youyi Wang are with the School of Electrical and Electronic Engineering, Nanyang Technological University, Singapore 639798 (e-mail: yuefei.zuo@ntu.edu.sg; chtlee@ntu.edu.sg; eyywang@ntu.edu.sg).

Color versions of one or more figures in this article are available at https://doi.org/10.1109/TPEL.2023.3262519.

Digital Object Identifier 10.1109/TPEL.2023.3262519

observer (PLLO) was employed in [13] to replace the linear ESO. Even if the PLLO-based ADRC system improves the low frequency disturbance rejection property, it sacrifices the medium frequency disturbance suppression performance at the same time, which deteriorates the robustness against inertia mismatch. With the rapid development of modern control theories, nonlinear control technique has been adopted to modify the conventional ESO [14], [15], [16]. The nonlinear function proposed by Han was employed in [16] to replace the linear function in conventional ESO. According to the range of tolerance to automatically adjust the gain of ESO, the estimation performance can be greatly improved. In [17], the generalized super-twisting algorithm was utilized to accelerate the convergence rate of the estimation error, which can optimize the performance of PMSM system. Besides, an adaptive linear/nonlinear switching ADRC method was proposed in [18] to maintain strong anti-disturbance property and high-precision tracking performance simultaneously. However, the switching mechanism is complex and defective.

Although the aforementioned ADRC systems have been widely applied in PMSM speed regulation system successfully, the research on the problem of smooth speed has been neglected. The speed fluctuation is affected by the torque ripple of motor, which is mainly caused by cogging torque and harmonic torque. To compensate for the disturbance at some specific frequencies in PMSM system, two quasi-resonant (QR) controllers were employed in [19] to suppress the first and second order harmonic components caused by offset error and scaling error. Unfortunately, the main harmonic component of torque ripple is not eliminated, which can be easily observed in the experimental results. Similarly, a combination of two vector resonant controllers and ADRC algorithm was utilized in [20] to replace the linear PI controller in current loop, which not only suppresses harmonic, but also improves resistance against system disturbance. Later, an adaptive ESO was constructed in [21] to enhance the measurement noise and torque ripple suppression performance without sacrificing the anti-disturbance capacity of PMSM speed regulation system. However, the control approach complicates the structure of ADRC method and the parameter tuning process.

Motivated by the discussions mentioned above, a nonlinear extended state observer (NESO) based modified ADRC (MADRC) scheme is proposed to optimize the robustness and disturbance rejection property of PMSM speed regulation system. By exploiting the finite time technique, the NESO with small bandwidth can achieve strong robustness, which greatly reduces the adverse effects of measurement noise on the closed-loop system. On this basis, a QR controller is combined with MADRC system to attenuate the main harmonic component of torque ripple for smooth speed. The contribution of this article could be briefly summarized in three aspects:

1) Utilizing the frequency-sweep method to obtain the bode diagrams of the MADRC algorithm with complex nonlinear terms, the advantages of the proposed control strategy can be clearly demonstrated in terms of frequency domain characteristics, which is more practical than traditional theoretical analysis from a mathematical point of view.
2) The proposed NESO adopts nonlinear functions to replace the linear terms in conventional ESO, thereby providing better resistance against low-medium frequency disturbance. In addition, the high frequency measurement noise can be effectively suppressed by utilizing a smaller observer bandwidth.
3) To reduce the speed fluctuation caused by undesired torque ripple, a QR controller is utilized to attenuate its main harmonic component for smooth speed. Combined the QR controller with the proposed MADRC method, the desired smooth speed and strong robustness can be achieved simultaneously.

II. Mathematical Model and Conventional ADRC Method

A. Modeling of PMSM System

The well-known motion equation of PMSM system can be described by [13]

$$\dot{\omega}_m = -\frac{B}{J}\omega_m + \frac{T_e}{J} - \frac{T_L}{J} \tag{1}$$

where ω_m is the rotor angular velocity, J is the moment of inertia, B is the viscous friction coefficient, T_L is the load torque, and T_e is the electromagnetic torque.

Taking the reference signal T_e^* as the control input, one obtains

$$\begin{aligned}\dot{\omega}_m &= \frac{T_e^*}{J} - \frac{B}{J}\omega_m - \left(\frac{T_e^*}{J} - \frac{T_e}{J}\right) - \frac{T_L}{J} \\ &= bT_e^* + d_0 \end{aligned} \tag{2}$$

where $b = \frac{1}{J}$ and $d_0 = -\frac{B}{J}\omega_m - \left(\frac{T_e^*}{J} - \frac{T_e}{J}\right) - \frac{T_L}{J}$ is the nominal disturbance.

Since the load torque is time-varying in practical engineering, the parameters of PMSM system may be mismatched. Compared to the viscous friction coefficient B, the value of inertia J may vary several times. As a result, the motion equation can be rewritten into a general form

$$\begin{aligned}\dot{\omega}_m &= b_0 T_e^* + (b - b_0)\, T_e^* + d_0 \\ &= b_0 T_e^* + d_t \end{aligned} \tag{3}$$

where $d_t = (b - b_0)T_e^* + d_0$ is the lumped disturbance, $b_0 = \frac{1}{J_0}$ and J_0 is the nominal value of inertia.

B. Conventional ADRC Algorithm Design

Defining the lumped disturbance d_t as an extended system state, the motion (3) can be rewritten as

$$\begin{cases}\dot{\omega}_m = b_0 T_e^* + d_t \\ \dot{d}_t = h\end{cases} \tag{4}$$

where h is the derivative of the lumped disturbance.

Generally, the conventional linear ESO is utilized to estimate the lumped disturbance d_t and mechanical angular velocity ω_m. However, it should be noted that the mechanical angular velocity is obtained by the derivative of the rotor position. As a matter of fact, the position signal is collected by position sensors, and

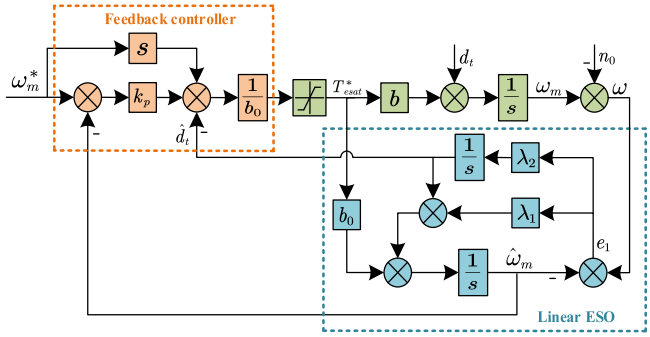

Fig. 1. Conventional ADRC algorithm for speed control.

the use of sensors will inevitably bring measurement noise, especially in the low speed region. Hence, the measured speed ω contained by measurement noise is given as

$$\omega = \omega_m - n_0 \tag{5}$$

where n_0 denotes the measurement noise.

According to [9], the conventional linear ESO for the system expressed by (3) can be designed as

$$\begin{cases} \dot{\hat{\omega}}_m = b_o T_e^* + \hat{d}_t + \lambda_1 e_1 \\ \dot{\hat{d}}_t = \lambda_2 e_1 \end{cases} \tag{6}$$

where $\hat{\omega}_m$ and $\hat{d}_t$ are the estimation of speed ω_m and disturbance d_t, λ_1 and λ_2 are the parameters of linear ESO and the estimation error $e_1 = \omega - \hat{\omega}_m$.

In order to facilitate the parameter tuning process, the observer gains can be given by

$$\begin{cases} \lambda_1 = 2p_0 \\ \lambda_2 = p_0^2 \end{cases} \tag{7}$$

where p_0 denotes the bandwidth related parameter of linear ESO.

After obtaining the estimation value of the lumped disturbance d_t and speed ω_m from linear ESO, the feedback controller can be constructed as

$$T_e^* = \frac{\dot{\omega}_m^* + k_p\left(\omega_m^* - \hat{\omega}_m\right) - \hat{d}_t}{b_0} \tag{8}$$

where k_p is the proportional gain. Moreover, Fig. 1 illustrates the block diagram of conventional ADRC system.

Remark 1: Obviously, the parameters k_p and p_0 determine the performance of ADRC method. The function of parameter k_p is similar to the proportional control in the conventional PI controller. Although increasing the value of parameter k_p can reduce the settling time when the motor speed changes, the peak value of the reference torque will inevitably increase, thereby generating actuator saturation. For parameter p_0, increasing the value of p_0 can enhance the disturbance rejection performance of the PMSM system. Unfortunately, the improvement of the disturbance rejection performance will inevitably lead to the degradation of the measurement noise suppression property.

Remark 2: Generally, the disturbance existing in PMSM system is in low-medium frequency band, while the measurement noise is in high frequency band. From the view of practical

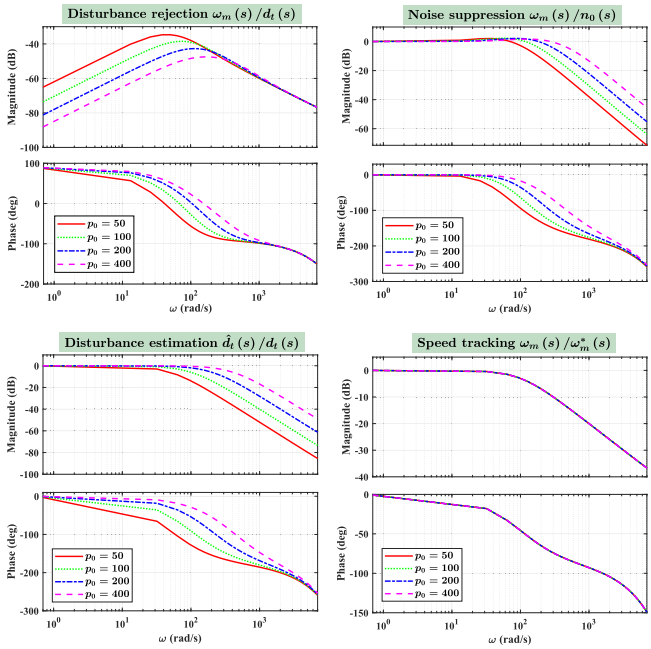

Fig. 2. Bode diagrams of conventional ADRC system under different p_0.

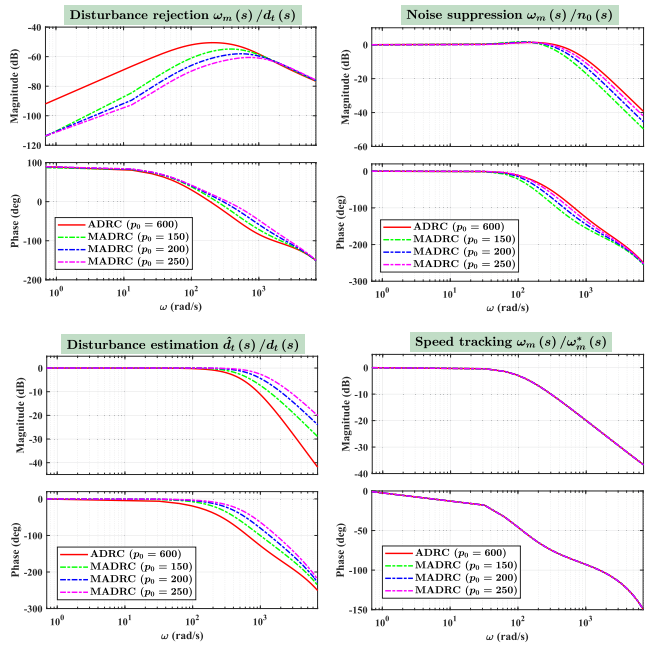

Fig. 3. Comparison of conventional ADRC and MADRC systems under different p_0.

engineering, only the bode diagrams of PMSM speed regulation system can clearly show its frequency domain characteristics. Since a novel NESO will be constructed in this article, and its transfer function is difficult to obtain. Therefore, a unified frequency-sweep method is adopted to acquire the bode diagrams of the conventional ADRC system and the upcoming MADRC system. Assuming the lumped disturbance as $d_t = A_0 \sin(\omega_f t)$, the rotor angular velocity ω_m nearly converges

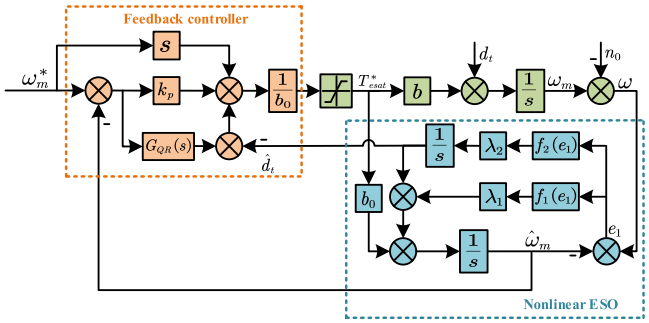

Fig. 4. Proposed QR-MADRC algorithm for speed control.

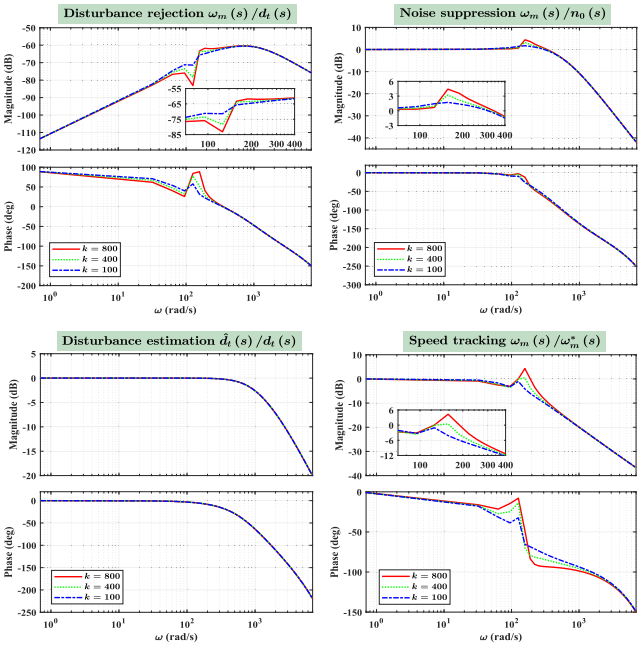

Fig. 5. Bode diagrams of QR-MADRC system under different k.

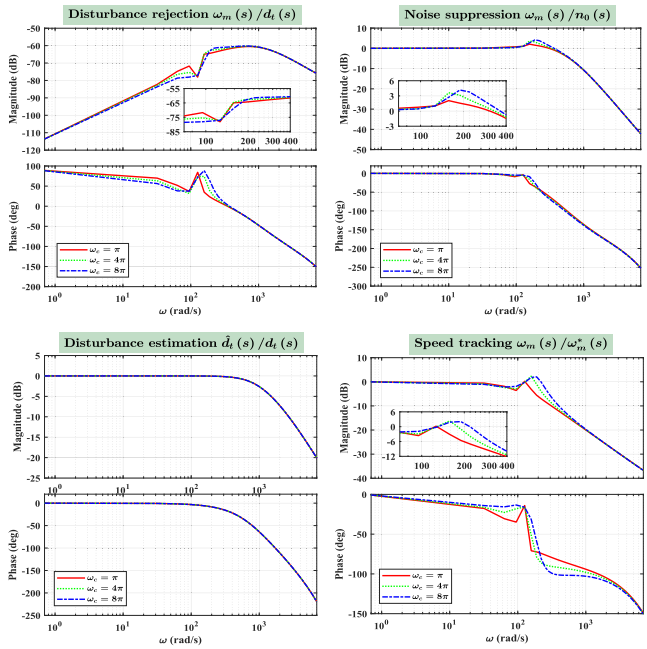

Fig. 6. Bode diagrams of QR-MADRC system under different ω_c.

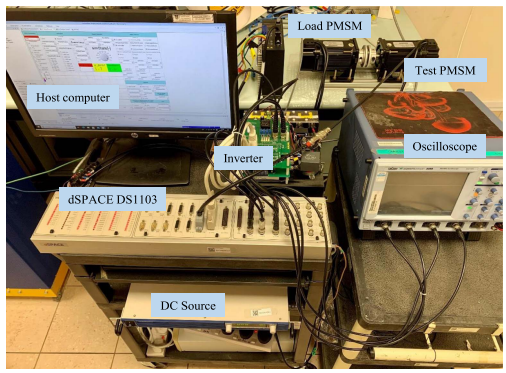

Fig. 7. Experimental platform.

to another sinusoidal function $\tilde{A}_0 \sin(\omega_f t + \varphi_f)$. On this basis, the magnitude frequency response and phase frequency response curves are given as $(\lg(\omega_f), 20\lg(\tilde{A}_0/A_0))$ and $(\lg(\omega_f), \varphi_f)$.

Selecting $b = b_0$ and $k_p = 100$, the bode diagrams of conventional ADRC system with variable p_0 is shown in Fig. 2. Since the lumped disturbance d_t is in low-medium frequency band, increasing the bandwidth of linear ESO can improve the disturbance estimation and rejection properties of the PMSM system. However, the larger p_0 is, the worse measurement noise suppression performance is. Consequently, the choice of parameter p_0 needs to find a balance between the above two factors.

III. Proposed Speed Loop Control Strategy

A. NESO Design

According to (3), the NESO can be constructed as

$$\begin{cases} \dot{\hat{\omega}}_m = b_0 T_e^* + \hat{d}_t + \lambda_1 f_1(e_1) \\ \dot{\hat{d}}_t = \lambda_2 f_2(e_1) \end{cases} \tag{9}$$

where nonlinear functions $f_1(e_1)$ and $f_2(e_1)$ are given as

$$\begin{aligned} f_1(e_1) &= \lfloor e_1 \rceil^{\gamma_1} + \lfloor e_1 \rceil^{\gamma_2} \\ f_2(e_1) &= \gamma_1 \lfloor e_1 \rceil^{2\gamma_1 - 1} + \gamma_2 \lfloor e_1 \rceil^{2\gamma_2 - 1} \\ &\quad + (\gamma_1 + \gamma_2) \lfloor e_1 \rceil^{\gamma_1 + \gamma_2 - 1} \end{aligned} \tag{10}$$

with $\gamma_1 = 1 + \alpha$, $\gamma_2 = 1 - \alpha$ and constant $\alpha \in (-\frac{1}{2}, 0)$. Notation $\lfloor \cdot \rceil^n$ represents $|\cdot|^n \cdot \mathrm{sign}(\cdot)$.

Subtracting (9) from (3), one obtains

$$\begin{cases} \dot{e}_1 = e_2 - \lambda_1 f_1(e_1) \\ \dot{e}_2 = -\lambda_2 f_2(e_1) - h \end{cases} \tag{11}$$

where $e_2 = d_t - \hat{d}_t$.

Remark 3: In the proposed NESO, the parameter α has a great influence on its performance. Decreasing the value of the parameter α can improve the estimation performance of NESO and promote the disturbance rejection property of the PMSM

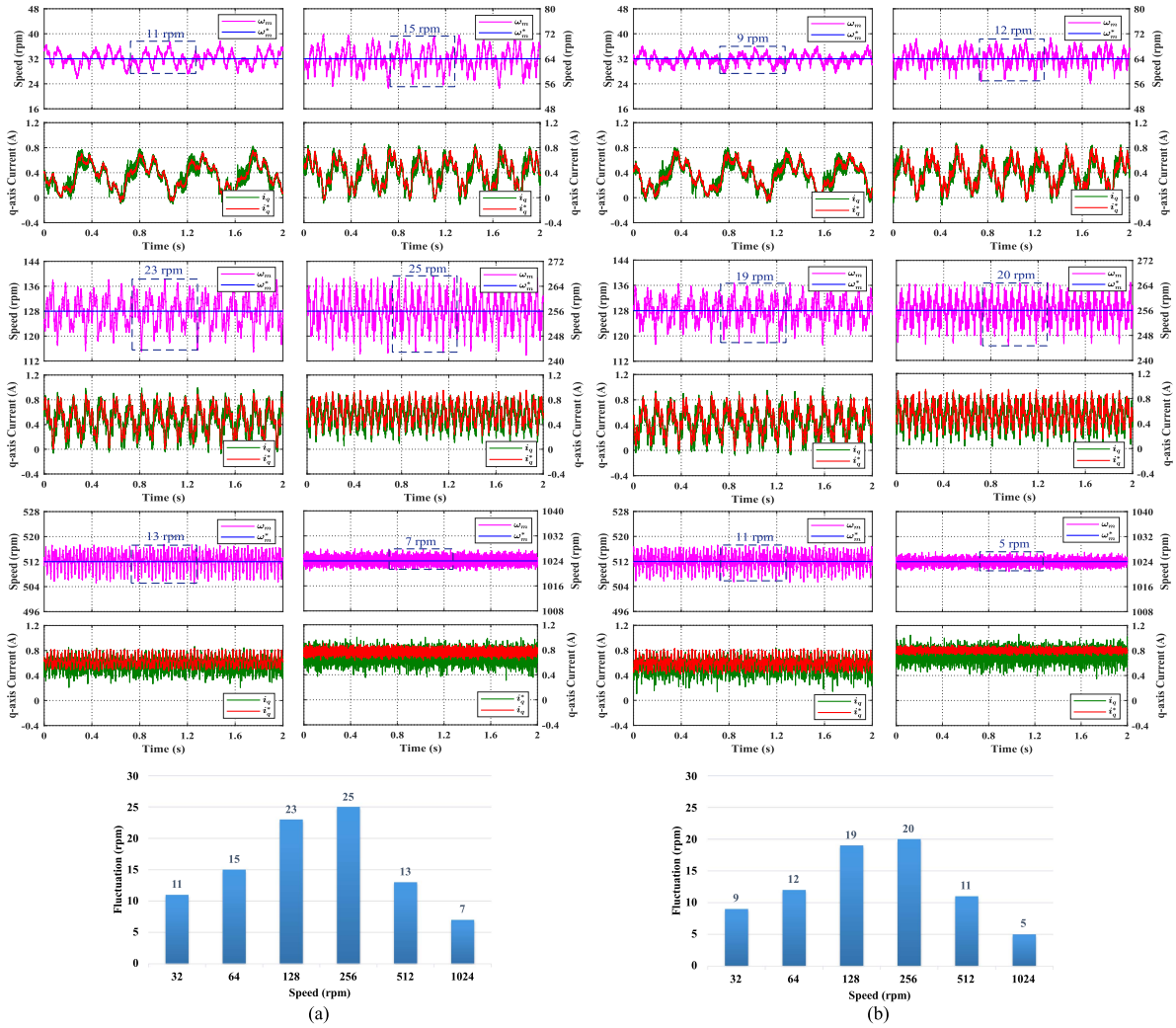

Fig. 8. Speed fluctuations of ADRC and MADRC methods under different speed regions. (a) ADRC. (b) MADRC.

system theoretically. Unfortunately, decreasing the value of α may enlarge the measurement noise in practical engineering. Hence, we need to choose an appropriate parameter α to achieve the desired performance. A simple and effective method for choosing an appropriate parameter α is to adjust parameter α from an initial large value to smaller values until the required performance is achieved.

Choosing $k_p = 100$, $b = b_0$ and $\alpha = -0.25$, the bode diagrams of MADRC system under different p_0 are shown in Fig. 3. Even if the value of parameter p_0 in MADRC system is smaller than conventional ADRC system, its low-medium frequency disturbance rejection ability is stronger. On this basis, the high frequency measurement noise suppression performance of MADRC system can be improved.

The estimation error of NESO will be shown to converge to zero in finite time. A widely used Lyapunov function is selected as

$$V = \xi^T Q \xi \tag{12}$$

where $\xi^T = [f_1(e_1), e_2]$ and Q is a positive definite symmetric matrix.

With the help of (10), one has

$$\dot{\xi} = F(e_1)(A\xi + B\vartheta) \tag{13}$$

where $F(e_1) = \gamma_1 |e_1|^{\gamma_1 - 1} + \gamma_2 |e_1|^{\gamma_2 - 1}$, $\vartheta = \frac{-h}{F(e_1)}$, $A = \begin{bmatrix} -\lambda_1 & 1 \\ -\lambda_2 & 0 \end{bmatrix}$ and $B = \begin{bmatrix} 0 \\ 1 \end{bmatrix}$.

Similar to [22], set $\Delta(\xi, \vartheta) = \begin{bmatrix} \xi \\ \vartheta \end{bmatrix}^T \begin{bmatrix} R & S^T \\ S & -\theta I \end{bmatrix} \begin{bmatrix} \xi \\ \vartheta \end{bmatrix}$, where $\theta \geqslant 0$. Then, the inequality $\Delta(\xi, \vartheta) \geqslant 0$ can be established with appropriate matrices R and S.

Theorem 1: If there exist a positive constant ε and positive definite symmetric matrix Q satisfying the following matrix inequality:

$$\begin{bmatrix} A^T Q + QA + \varepsilon Q + R & QB + S^T \\ B^T Q + S & -\theta I \end{bmatrix} \leqslant 0$$

then the estimation error system (11) is finite time stable.

Proof: By a simple calculation, the derivative of V is

$$\dot{V} = F(e_1)\left[\xi^T \left(A^T Q + QA\right)\xi + \vartheta B^T Q \xi + \xi^T Q B \vartheta\right]$$

$$= F(e_1)\begin{bmatrix}\xi\\ \vartheta\end{bmatrix}^T\begin{bmatrix}A^TQ+QA & QB\\ B^TQ & 0\end{bmatrix}\begin{bmatrix}\xi\\ \vartheta\end{bmatrix}. \tag{14}$$

Since $\|\xi\|^2 = |e_1|^{2\gamma_1} + |e_1|^{2\gamma_2} + 2|e_1|^{\gamma_1+\gamma_2} + |e_2|^2$, $0 < \frac{1-\gamma_1}{\gamma_1} < 1$, and the inequality $\lambda_{\min}\{Q\}\|\xi\|^2 \leqslant \xi^TQ\xi \leqslant \lambda_{\max}\{Q\}\|\xi\|^2$ holds, one has

$$\left(|e_1|^{\gamma_1}\right)^{\frac{1-\gamma_1}{\gamma_1}} \leqslant \left(\frac{V^{\frac{1}{2}}}{\lambda_{\min}^{\frac{1}{2}}\{Q\}}\right)^{\frac{1-\gamma_1}{\gamma_1}}. \tag{15}$$

With the help of (15) and $\Delta(\xi,\vartheta) \geqslant 0$, (14) can be rewritten as

$$\begin{aligned}\dot V &\leqslant F(e_1)\left\{\begin{bmatrix}\xi\\ \vartheta\end{bmatrix}^T\begin{bmatrix}A^TQ+QA & QB\\ B^TQ & 0\end{bmatrix}\begin{bmatrix}\xi\\ \vartheta\end{bmatrix} + \Delta(\xi,\vartheta)\right\}\\ &\leqslant F(e_1)\begin{bmatrix}\xi\\ \vartheta\end{bmatrix}^T\begin{bmatrix}-\varepsilon Q & 0\\ 0 & 0\end{bmatrix}\begin{bmatrix}\xi\\ \vartheta\end{bmatrix}\\ &\leqslant -\gamma_1|e_1|^{\gamma_1-1}\varepsilon V\\ &= -\frac{\gamma_1}{|e_1|^{1-\gamma_1}}\varepsilon V\\ &\leqslant -\gamma_1\lambda_{\min}^{\frac{1-\gamma_1}{2\gamma_1}}\{Q\}\varepsilon V^{\frac{3\gamma_1-1}{2\gamma_1}}.\end{aligned} \tag{16}$$

Obviously, (16) satisfies the finite-time stability criterion in [23]. Therefore, the estimation error system (11) can be stabilized in a finite time. ■

B. QR-MADRC Design

In order to obtain the smooth speed, the QR controller is employed in this section to attenuate the main harmonic component of torque ripple caused by some undesired factors during the motor manufacturing process. According to [19], the transfer function of QR controller can be expressed as

$$G_{QR}(s) = \frac{2k\omega_c s}{s^2 + 2\omega_c s + \omega_0^2} \tag{17}$$

where k is the resonant coefficient, ω_c and ω_0 are the cutoff frequency and resonant frequency of QR controller, respectively. Combined with the aforementioned NESO, the block diagram of the proposed QR-MADRC algorithm is shown in Fig. 4.

Choosing $\omega_0 = 40\pi$ rad/s and $\omega_c = 2\pi$ rad/s, the bode diagrams of QR-MADRC system under different parameter k are shown in Fig. 5. It can be clearly seen that the QR controller provides additional disturbance rejection property at resonant frequency ω_0, which can suppress the harmonic component at ω_0 effectively. The stronger disturbance rejection property can be achieved by increasing the value of resonant coefficient k. In addition, selecting $\omega_0 = 40\pi$ rad/s and $k = 350$, the bode diagrams of QR-MADRC system under different parameter ω_c are shown in Fig. 6. Increasing the value of cutoff frequency ω_c can expand the influence range of the QR controller on the entire PMSM speed regulation system.

Remark 4: According to the frequency domain characteristics of QR-MADRC system, it is convenient to obtain the desired control performance. First of all, an appropriate resonant coefficient k should be selected to increase the disturbance rejection property at resonant frequency ω_0, so that the torque ripple can be well suppressed. In addition, adjusting the cutoff frequency ω_c can alter the influence region of QR controller around ω_0. However, the introduction of QR controller will adversely affect the noise suppression and speed tracking performance of the PMSM speed regulation system. Considering the above factors simultaneously, the parameters of QR controller have to be chosen in a compromise way.

TABLE I
MAIN PARAMETERS OF THE PMSM SYSTEM

Parameter	Symbol	Value and Unit
Number of pole pairs	p_n	4
Stator resistance	R_s	1.1 Ω
Stator inductance	L_s	5.7 mH
Permanent-magnet flux linkage	φ_f	0.092 wb
Rated power	P_N	0.75 kW
Rated speed	n_N	3000 rpm
Rated voltage	U_n	220 V
Rated torque	T_N	2.4 N·m
Moment of inertia	J	1.62×10^{-4} kg/m^2
Control period	T	100 μs

IV. EXPERIMENTAL RESULTS

In order to demonstrate the effectiveness of the proposed control scheme, experiments are carried out on the test bench based on dSPACE DS1103. The experimental platform is shown in Fig. 7, and the corresponding technical parameters are given in Table I. The platform employs two identical 0.75 kW motors, one acts as a test motor and the other acts as a load torque generator. The field-oriented control with $i_d^* = 0$ is adopted as the basic control strategy, and the control frequency is synchronized to 10 kHz.

A. Comparative Results of Conventional ADRC and MADRC

The performance of conventional ADRC and proposed MADRC schemes are compared in this section. The proportional gain of these two methods are the same, i.e., $k_p = 100$. The values of parameter p_0 in ESO and NESO are chosen as 600 and 250, respectively. The parameter α in NESO is selected as -0.25.

In order to verify the validity of the frequency-sweep analysis method, the reference speed of the geometric progression is employed to show the disturbance rejection performance of conventional ADRC and proposed MADRC strategies. The corresponding experimental results are shown in Fig. 8. Obviously, the speed fluctuation in the medium frequency band is large, that is, the disturbance rejection performance of PMSM system in the medium frequency band is unsatisfactory, which is consistent with the results of frequency-sweep method. Furthermore, the speed fluctuation under the proposed MADRC method is always smaller than the conventional ADRC scheme.

To demonstrate the speed tracking performance of conventional ADRC and proposed MADRC methods, typical sinusoidal reference is given. The corresponding experimental results are presented in Fig. 9. It can be easily observed that the

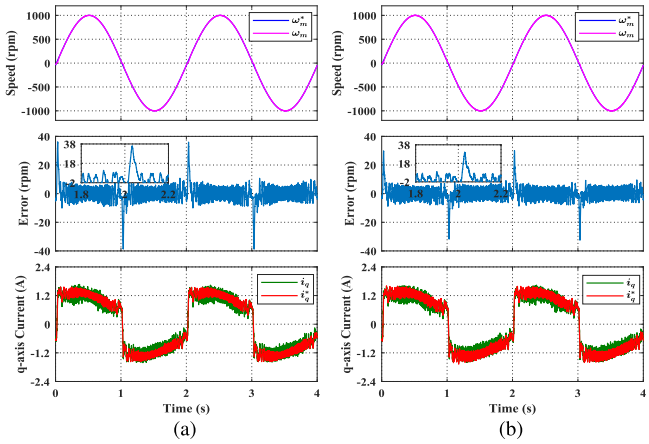

Fig. 9. Tracking performance of ADRC and MADRC methods under sinusoidal reference. (a) ADRC. (b) MADRC.

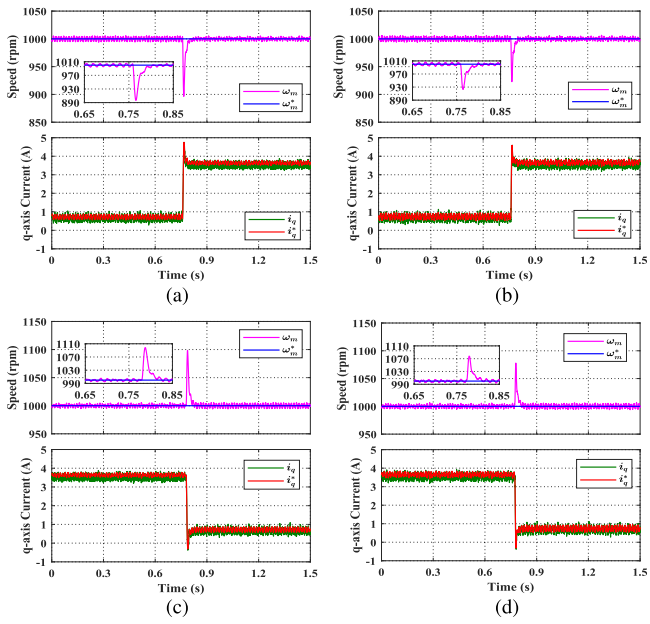

Fig. 10. Disturbance rejection performance of ADRC and MADRC methods. (a) ADRC under step loading. (b) MADRC under step loading. (c) ADRC under step unloading. (d) MADRC under step unloading.

tracking error of MADRC for sinusoidal reference is smaller than that of ADRC. In addition, the experimental results of conventional ADRC and proposed MADRC strategies under step loading and unloading are illustrated in Fig. 10. For the conventional ADRC method, the speed drop under step loading and the speed rise under step unloading are 104 rpm and 98 rpm, respectively. Meanwhile, for the proposed MADRC method, the speed drop under step loading and the speed rise under step unloading is 77 rpm and 75 rpm, respectively. It can be concluded that the disturbance rejection ability of MADRC is stronger than the conventional ADRC strategy. Fig. 11 shows the robustness of conventional ADRC and proposed MADRC algorithms under inertia mismatch. According to the experimental results in Fig. 11, the motor under conventional ADRC strategy has more obvious oscillation phenomenon. Hence, it

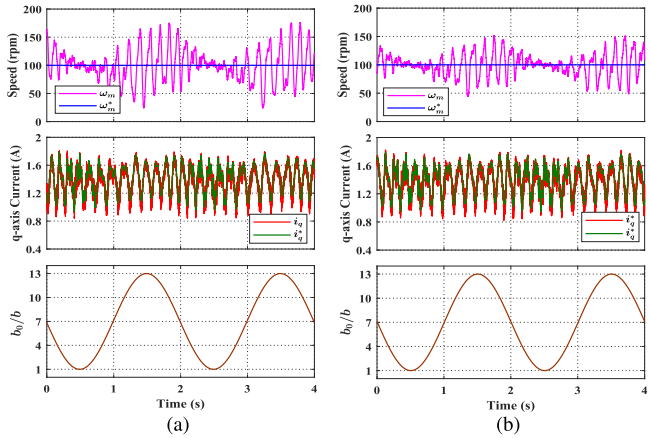

Fig. 11. Robustness of ADRC and MADRC methods under inertia mismatch. (a) ADRC. (b) MADRC.

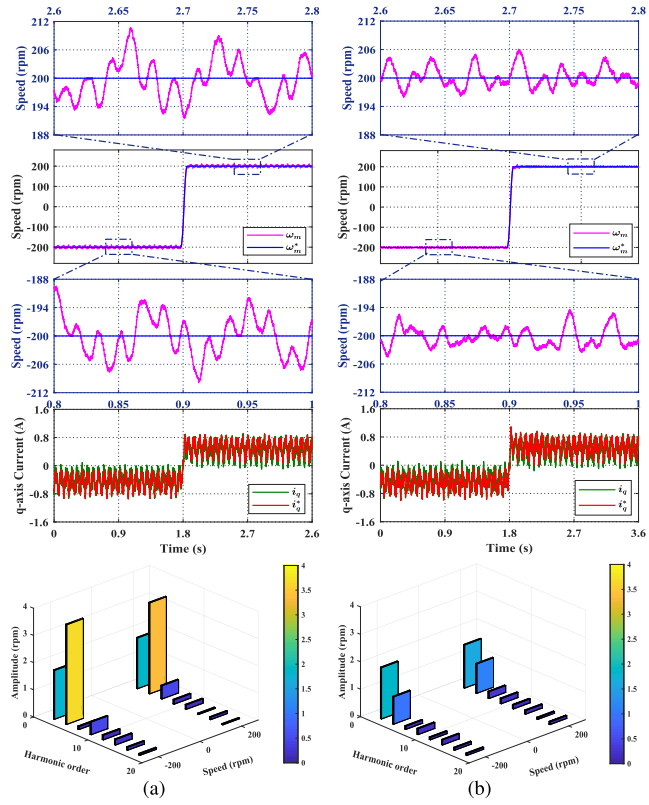

Fig. 12. Torque ripple suppression performance of QR-MADRC method. (a) MADRC. (b) QR-MADRC.

can be easily observed that the proposed MADRC can provide stronger robustness in the presence of inertia mismatch.

B. *Torque Ripple Suppression of QR-MADRC*

The speed fluctuation is affected by the torque ripple caused by some undesired factors during the motor manufacturing process, especially in low speed region. For this reason, a square wave reference speed ranging from -100 rpm to 100 rpm is adopted to clearly show the effect of QR controller on harmonic

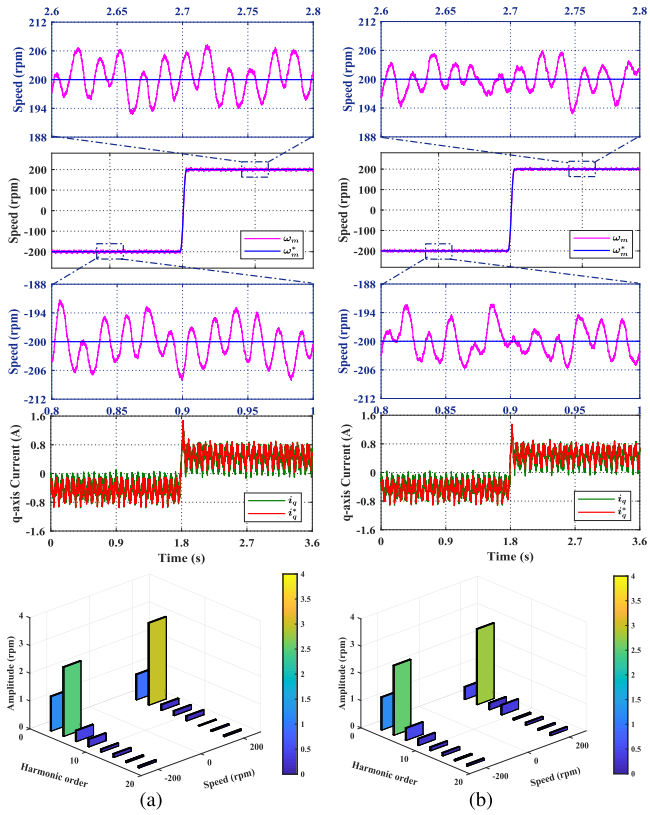

Fig. 13. Torque ripple suppression performance of QR-MADRC method with incorrect resonant frequency. (a) $\omega_0 = 4\omega_e$. (b) $\omega_0 = 5\omega_e$.

suppression in this section. Fig. 12(a) depicts the speed response of the proposed MADRC method, and the main harmonic component of torque ripple is the 4.5th-order harmonic. In order to attenuate the biggest harmonic of the torque ripple, the resonant frequency of QR controller is chosen as $\omega_0 = 4.5\omega_e$, where ω_e is the electrical angular speed. According to the Fourier analysis of the steady-state speed, it can be observed that the QR controller can effectively attenuate the 4.5th-order harmonic. Therefore, the speed fluctuation phenomenon caused by torque ripple can be greatly reduced.

Meanwhile, in order to demonstrate the robustness of the QR controller, the experimental results of the proposed QR-MADRC strategy with incorrect resonant frequency are illustrated in Fig. 13. When the resonant frequency is selected as $\omega_0 = 4\omega_e$ or $\omega_0 = 5\omega_e$, the QR controller can still attenuate the 4.5th-order harmonic to a certain extent. It can be concluded that the QR controller is insensitive to the resonant frequency and it has a satisfactory disturbance rejection ability.

V. Conclusion

In this article, a QR-MADRC strategy is proposed to achieve strong robustness and smooth speed of PMSM speed regulation system. Compared with the conventional ESO, the proposed NESO can take advantage of finite-time technique to provide strong robustness and disturbance rejection ability. Meanwhile, a QR controller is adopted to suppress the main harmonic component of torque ripple for smooth speed. Frequency-sweep analysis and experimental results demonstrate that the proposed QR-MADRC method outperforms conventional ADRC approach. Our future work will focus on improving the control performance of the proposed scheme at low switching frequency.

References

[1] Z. Li, F. X. Wang, D. L. Ke, J. X. Li, and W. Zhang, "Robust continuous model predictive speed and current control for PMSM with adaptive integral sliding-mode approach," *IEEE Trans. Power Electron.*, vol. 36, no. 12, pp. 14398–14408, Dec. 2021.

[2] Q. K. Hou, S. H. Ding, and X. H. Yu, "Composite super-twisting sliding mode control design for PMSM speed regulation problem based on a novel disturbance observer," *IEEE Trans. Energy Convers.*, vol. 36, no. 4, pp. 2591–2599, Dec. 2021.

[3] S. D. Zhu, W. X. Zhao, G. H. Liu, Y. X. Mao, and Y. H. Sun, "Effect of phase shift angle on radial force and vibration behavior in dual three-phase PMSM," *IEEE Trans. Ind. Electron.*, vol. 68, no. 4, pp. 2988–2998, Apr. 2021.

[4] L. Ma, K. Q. Mei, S. H. Ding, and T. H. Pan, "Design of adaptive fuzzy fixed-time HOSM controller subject to asymmetric output constraints," *IEEE Trans. Fuzzy Syst.*, early access, Jan. 31, 2023, doi: 10.1109/TFUZZ.2023.3241147.

[5] Q. K. Hou and S. H. Ding, "Generalized proportional integral observer based super-twisting sliding mode control for PMSM," *IEEE Trans. Circuits Syst. II, Exp. Briefs*, vol. 68, no. 2, pp. 747–751, Jul. 2020.

[6] Q. K. Hou, S. H. Ding, X. H. Yu, and K. Q. Mei, "A super-twisting-like fractional controller for SPMSM drive system," *IEEE Trans. Ind. Electron.*, vol. 69, no. 9, pp. 9376–9384, Sep. 2022.

[7] S. H. Ding, W. H. Chen, K. Q. Mei, and D. J. Murray-Smith, "Disturbance observer design for nonlinear systems represented by input-output models," *IEEE Trans. Ind. Electron.*, vol. 67, no. 2, pp. 1222–1232, Feb. 2020.

[8] J. Q. Han, "From PID to active disturbance rejection control," *IEEE Trans. Ind. Electron.*, vol. 56, no. 3, pp. 900–906, Mar. 2009.

[9] R. Zhou, C. F. Fu, and W. Tan, "Implementation of linear controllers via active disturbance rejection control structure," *IEEE Trans. Ind. Electron.*, vol. 68, no. 7, pp. 6217–6226, Jul. 2021.

[10] S. L. Li, X. Yang, and D. Yang, "Active disturbance rejection control for high pointing accuracy and rotation speed," *Automatica*, vol. 45, no. 8, pp. 1854–1860, Aug. 2009.

[11] S. H. Li and Z. G. Liu, "Adaptive speed control for permanent-magnet synchronous motor system with variations of load inertia," *IEEE Trans. Ind. Electron.*, vol. 56, no. 8, pp. 3050–3059, Aug. 2009.

[12] W. Xu, R. J. Dian, Y. Liu, D. Hu, and J. G. Zhu, "Robust flux estimation method for linear induction motors based on improved extended state observers," *IEEE Trans. Power Electron.*, vol. 34, no. 5, pp. 4628–4640, May 2019.

[13] Y. F. Zuo, X. Y. Zhu, Q. Li, C. Zhang, Y. Du, and Z. X. Xiang, "Active disturbance rejection controller for speed control of electrical drives using phase-locking loop observer," *IEEE Trans. Ind. Electron.*, vol. 66, no. 3, pp. 1748–1759, Mar. 2019.

[14] L. Zhao, X. Liu, and T. Wang, "Trajectory tracking control for double-joint manipulator systems driven by pneumatic artificial muscles based on a nonlinear extended state observer," *Mech. Syst. Signal Process.*, vol. 122, pp. 307–320, May 2019.

[15] L. Zhang, C. Z. Wei, R. Wu, and N. G. Cui, "Fixed-time extended state observer based non-singular fast terminal sliding mode control for a VTVL reusable launch vehicle," *Aerosp. Sci. Technol.*, vol. 82-83, pp. 70–79, Nov. 2018.

[16] L. H. Zhu et al., "Nonlinear active disturbance rejection control strategy for permanent magnet synchronous motor drives," *IEEE Trans. Energy Convers.*, vol. 37, no. 3, pp. 2119–2129, Sep. 2022.

[17] Q. K. Hou and S. H. Ding, "Finite-time extended state observer based super-twisting sliding mode controller for PMSM drives with inertia identification," *IEEE Trans. Transp. Electrific.*, vol. 8, no. 2, pp. 1918–1929, Jun. 2022.

[18] Z. J. Hao et al., "Linear/nonlinear active disturbance rejection switching control for permanent magnet synchronous motors," *IEEE Trans. Power Electron.*, vol. 36, no. 8, pp. 9334–9347, Aug. 2021.

[19] B. Wang, M. H. Tian, Y. Yong, Q. H. Dong, and D. G. Xu, "Enhanced ADRC with quasi-resonant control for PMSM speed regulation considering aperiodic and periodic disturbances," *IEEE Trans. Transp. Electrific.*, vol. 8, no. 3, pp. 3568–3577, Sep. 2022.
[20] Z. Wang, J. W. Zhao, L. J. Wang, M. Li, and Y. P. Hu, "Combined vector resonant and active disturbance rejection control for PMSLM current harmonic suppression," *IEEE Trans. Ind. Inform.*, vol. 16, no. 9, pp. 5691–5702, Sep. 2020.
[21] S. F. Zhu et al., "Robust speed control of electrical drives with reduced ripple using adaptive switching high-order extended state observer," *IEEE Trans. Power Electron.*, vol. 37, no. 2, pp. 2009–2020, Feb. 2022.
[22] L. Zhao, S. M. Gu, J. H. Zhang, and S. H. Li, "Finite-time trajectory tracking control for rodless pneumatic cylinder systems with disturbances," *IEEE Trans. Ind. Electron.*, vol. 69, no. 4, pp. 4137–4147, Apr. 2022.
[23] S. H. Yu, X. H. Yu, B. Shirinzadeh, and Z. H. Man, "Continuous finite-time control for robotic manipulators with terminal sliding mode," *Automatica*, vol. 41, no. 11, pp. 1957–1964, Nov. 2005.

Qiankang Hou was born in Jiangsu, China, in 1995. He is currently working toward the Ph.D. degree in control science and engineering with the School of Electrical and Information Engineering, Jiangsu University, Zhenjiang, China.

From 2021 to 2022, he was financially supported by the China Scholarship Council to work as a Visiting Ph.D. Student with the School of Electrical and Electronic Engineering, Nanyang Technological University, Singapore. His research interests include nonlinear control and its application to permanent magnet synchronous motor servo systems.

Yuefei Zuo (Member, IEEE) received the B.Sc. and the Ph.D. degrees in electrical engineering and automation from the Nanjing University of Aeronautics and Astronautics, Nanjing, China, in 2010 and 2016, respectively.

From 2016 to 2019, he was a Lecturer with the School of Electrical and Information Engineering, Jiangsu University, Zhenjiang, China. He is currently a Senior Research Fellow with the School of Electrical and Electronic Engineering, Nanyang Technological University, Singapore. His research interests include power electronics, electric machines and drives, and advanced control strategies.

Jinlin Sun received the B.Eng. degree in automation from Jiangsu University, Zhenjiang, China, in 2016, and the Ph.D. degree in control theory and control engineering from the Institute of Automation, Chinese Academy of Sciences, Beijing, China, in 2021.

He is currently a Lecturer with the School of Electrical and Information Engineering, Jiangsu University, Zhenjiang, China. From October 2019 to October 2020, he visited the Department of Electrical, Computer, and Biomedical Engineering, University of Rhode Island, Kingston, RI, USA. His current research interests include anti-disturbance control, robust adaptive control, and their applications.

Christopher H. T. Lee (Senior Member, IEEE) received the B.Eng. (First Class Hons.) and Ph.D. degrees both in electrical engineering from the Department of Electrical and Electronic Engineering, The University of Hong Kong, Hong Kong, in 2009 and 2016, respectively.

He is currently an Assistant Professor with Nanyang Technological University, Singapore, a Visiting Assistant Professor with Massachusetts Institute of Technology, USA, and also a Honorary Assistant Professor with The University of Hong Kong, Hong Kong. He is an Associate Editor for IEEE TRANSACTIONS ON INDUSTRIAL ELECTRONICS, IEEE TRANSACTIONS ON ENERGY CONVERSION, IEEE ACCESS, and *IET Renewable Power Generation*. His research interests include electric machines and drives, renewable energies, and electromechanical propulsion technologies. In these areas, he has published 1 book, 3 books chapters, and over 80 referred papers.

Dr. Lee has received many awards, including NRF Fellowship, Nanyang Assistant Professorship, Li Ka Shing Prize (the best Ph.D. thesis prize), and Croucher Foundation Fellowship.

Youyi Wang received the B.Eng. degree from the Beijing University of Science and Technology, Beijing, China, in 1982, the M.Eng. degree from Tsinghua University, Beijing, in 1984, and the Ph.D. degree from the University of Newcastle, Callaghan, NSW, Australia, in 1991, all in electrical engineering.

In 1991, he joined Nanyang Technological University, Singapore, Singapore, where he is currently a Professor with the School of Electrical and Electronic Engineering. His main research interests include nonlinear control, robust control, control and applications of control theory to power systems, electric drive systems, and information storage systems.

Dr. Wang is currently a Senior Member of the IEEE Control Systems Society and the IEEE Power Engineering Society.

Shihong Ding (Member, IEEE) was born in Anhui, China, in 1983. He received the B.E. degree in mathematics from Anhui Normal University, Anhui, China, in 2004, and the M.S. and Ph.D. degrees in automatic control from Southeast University, Nanjing, China, in 2007 and 2010, respectively.

During the graduate studies, he visited The University of Texas at San Antonio from August 2008 to August 2009. After graduation, he held a research fellowship with the University of Western Sydney for one year. He also visited Yeungnam University, South Korea, from July 2018 to August 2018 and RMIT University, from December 2019 to February 2020, respectively. Since June 2010, he has been with the School of Electrical and Information Engineering, Jiangsu University, where he is currently a Full Professor. His research interests include sliding mode control and finite-time stability. He currently serves as a Subject Editor of nonlinear dynamics and an Associate Editor of IEEE ACCESS.